Autotaxin expression from synovial fibroblasts is essential for the pathogenesis of modeled arthritis

Nikitopoulou, Ioanna ; Oikonomou, Nikos ; Karouzakis, Emmanuel ; Sevastou, Ioanna ; Nikolaidou-Katsaridou, Nefeli ; Zhao, Zhenwen ; Mersinias, Vassilis ; Armaka, Maria ; Xu, Yan ; Masu, Masayuki ; Mills, Gordon B ; Gay, Steffen ; Kollias, George ; Aidinis, Vassilis

Abstract: Rheumatoid arthritis is a destructive arthropathy characterized by chronic synovial inflammation that imposes a substantial socioeconomic burden. Under the influence of the proinflammatory milieu, synovial fibroblasts (SFs), the main effector cells in disease pathogenesis, become activated and hyperplastic, releasing proinflammatory factors and tissue-remodeling enzymes. This study shows that activated arthritic SFs from human patients and animal models express significant quantities of autotaxin (ATX; ENPP2), a lysophospholipase D that catalyzes the conversion of lysophosphatidylcholine to lysophosphatidic acid (LPA). ATX expression from SFs was induced by TNF, and LPA induced SF activation and effector functions in synergy with TNF. Conditional genetic ablation of ATX in mesenchymal cells, including SFs, resulted in disease attenuation in animal models of arthritis, establishing the ATX/LPA axis as a novel player in chronic inflammation and the pathogenesis of arthritis and a promising therapeutic target.

DOI: https://doi.org/10.1084/jem.20112012

Published April 9, 2012

Autotaxin expression from synovial fibroblasts is essential for the pathogenesis of modeled arthritis

Ioanna Nikitopoulou,[1] Nikos Oikonomou,[1] Emmanuel Karouzakis,[2] Ioanna Sevastou,[1] Nefeli Nikolaidou-Katsaridou,[1] Zhenwen Zhao,[3] Vassilis Mersinias,[1] Maria Armaka,[1] Yan Xu,[3] Masayuki Masu,[4] Gordon B. Mills,[5] Steffen Gay,[2] George Kollias,[1] and Vassilis Aidinis[1]

[1]Institute of Immunology, Alexander Fleming Biomedical Sciences Research Center, 16672 Athens, Greece
[2]Center of Experimental Rheumatology, University Hospital Zurich, CH-8091 Zurich, Switzerland
[3]Department of Obstetrics and Gynecology, Indiana University School of Medicine, Indianapolis, IN 46202
[4]Department of Molecular Neurobiology, Graduate School of Comprehensive Human Sciences, University of Tsukuba, Tsukuba, Ibaraki 305-8575, Japan
[5]Department of Systems Biology, The University of Texas MD Anderson Cancer Center, Houston, TX 77030

Rheumatoid arthritis is a destructive arthropathy characterized by chronic synovial inflammation that imposes a substantial socioeconomic burden. Under the influence of the proinflammatory milieu, synovial fibroblasts (SFs), the main effector cells in disease pathogenesis, become activated and hyperplastic, releasing proinflammatory factors and tissue-remodeling enzymes. This study shows that activated arthritic SFs from human patients and animal models express significant quantities of autotaxin (ATX; ENPP2), a lysophospholipase D that catalyzes the conversion of lysophosphatidylcholine to lysophosphatidic acid (LPA). ATX expression from SFs was induced by TNF, and LPA induced SF activation and effector functions in synergy with TNF. Conditional genetic ablation of ATX in mesenchymal cells, including SFs, resulted in disease attenuation in animal models of arthritis, establishing the ATX/LPA axis as a novel player in chronic inflammation and the pathogenesis of arthritis and a promising therapeutic target.

CORRESPONDENCE
Vassilis Aidinis:
V.Aidinis@Fleming.gr

Abbreviations used: Ab, antibody; ATX, autotaxin; CIA, collagen-induced arthritis; HRP, horseradish peroxidase; LC/MS, liquid chromatography mass spectrometry; LPA, lysophosphatidic acid; LPAR, LPA receptor; LPC, lysophosphatidylcholine; mRNA, messenger RNA; OA, osteoarthritis; P4H, prolyl 4-hydroxylase; Q-RT-PCR, quantitative RT-PCR; RA, rheumatoid arthritis; SF, synovial fibroblast.

Rheumatoid arthritis (RA) pathogenesis is characterized by a hyperplastic synovial membrane caused by synovial cell proliferation and infiltration by inflammatory cells (Müller-Ladner et al., 2005). Synovial fibroblasts (SFs) are among the dominant cell types of the arthritic synovium that under the influence of the inflammatory milieu and/or possible epigenetic changes become activated and hyperplastic, releasing several effector signals including proinflammatory factors and tissue-remodeling enzymes (Karouzakis et al., 2009).

Autotaxin (ATX) is a secreted lysophospholipase D, widely present in biological fluids, catalyzing the conversion of lysophosphatidylcholine (LPC) to lysophosphatidic acid (LPA; Aoki, 2004; van Meeteren and Moolenaar, 2007). LPA evokes growth factor–like responses in almost all cell types, including cell growth, survival, differentiation, and motility (Mills and Moolenaar, 2003). The wide variety of LPA effector functions is attributed to at least five G-protein–coupled LPA receptors (LPARs) with overlapping specificities and widespread distribution (Choi et al., 2008).

Increased ATX expression has been detected in a large variety of cancers (van Meeteren and Moolenaar, 2007); in this study, substantial ATX expression is detected from SFs in arthritic joints of animal models and human patients. Conditional genetic ablation of ATX in SFs (and other mesenchymal cells) is shown to attenuate disease pathogenesis, attributed to diminished LPA signaling to SFs.

The Rockefeller University Press $30.00
J. Exp. Med. Vol. 209 No. 5 925-933
www.jem.org/cgi/doi/10.1084/jem.20112012

Supplemental Material can be found at:
http://jem.rupress.org/content/suppl/2012/04/05/jem.20112012.DC1.html

Published April 9, 2012

RESULTS AND DISCUSSION

Increased, TNF-driven ATX expression from SFs in mouse arthritic joints

Increased ATX messenger RNA (mRNA) expression has been previously detected through differential expression profiling in primary arthritic mouse SFs isolated from an animal model of inflammatory arthritis (Aidinis et al., 2005), confirmed here with quantitative RT-PCR (Q-RT-PCR; not depicted). No ATX mRNA expression was detected in primary immune cells even upon their activation (not depicted), an observation consistent with the expression of other ENPP family members in these cell types (Stefan et al., 2005; van Meeteren and Moolenaar, 2007). Immunostaining of ex vivo cultured primary SFs further confirmed the increased ATX expression in arthritic ($hTNF^{+/-}$) SFs (Fig. 1 a). Accordingly, ATX was also detected in SF supernatants, where arthritic SFs were found to secrete significantly more ATX than WT SFs (Fig. 1, b and c). The increased ATX expression in arthritic SFs was also confirmed by FACS analysis (not depicted), which further indicated that the vast majority of ATX-expressing cultured cells were fibroblasts (vimentin$^+$) and that both intimal (VCAM$^+$) and subintimal (VCAM$^-$) SFs (Edwards, 2000) express ATX (Fig. 1 d). Moreover, TNF, the major proinflammatory cytokine that drives disease development in this animal model, was shown to induce ATX expression from WT SFs ex vivo, both at the mRNA (Fig. 1 e) and protein level (intracellular or secreted; Fig. 1, f and g, respectively), most likely through an NF-κB–dependent mechanism (Zhao et al., 2008). Previous studies have also suggested modulation of ATX expression from other cytokines (Santos et al., 1996; Kehlen et al., 2001), although more detailed studies are needed.

To validate the results in vivo, immunostaining was used to assess ATX expression in the arthritic joints of three animal models of arthritis (Kollias et al., 2011): two inflammatory driven by TNF overexpression, the $hTNF^{+/-}$ transgenic (Keffer et al., 1991) and the $Tnf^{\Delta ARE/+}$ knockin (Kontoyiannis et al., 1999), and one autoimmune, collagen-induced arthritis (CIA; Campbell et al., 2000). In all models, substantial ATX expression was detected in the synovial tissue of inflamed joints compared with the almost complete absence of staining in WT control joints (Fig. 2, a and b). In accordance with the ex vivo results, ATX staining was localized in SFs, as shown with immunostaining for vimentin in sequential joint sections from $hTNF^{+/-}$ mice (Fig. 2 c and Fig. S1, a and d). Constitutive ATX expression was also noted in chondrocytes, in line with its suggested role in mesenchymal development as a Bmp-2 downstream target (Bächner et al., 1998); however, their relative contribution to the synovium ATX levels is negligible in comparison with the activated SFs in the hyperplastic synovial membrane.

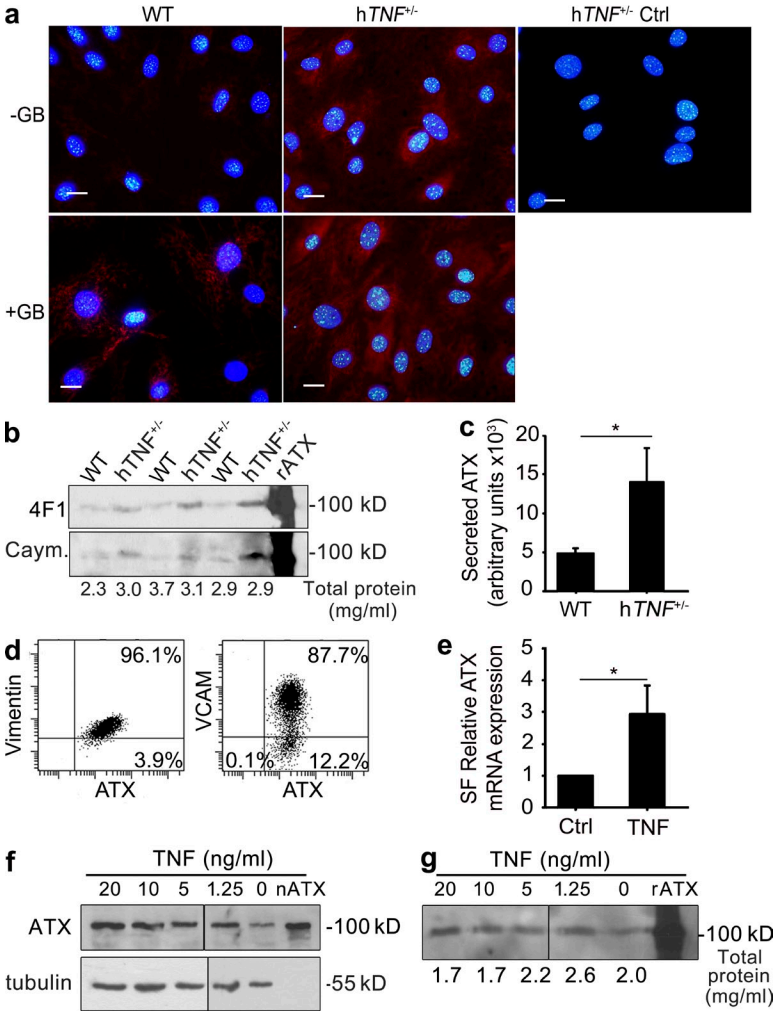

Figure 1. Increased ATX expression in arthritic ($hTNF^{+/-}$) primary mouse SFs. (a) SFs from WT and $hTNF^{+/-}$ littermate mice were cultured and stained for ATX (red) and nuclei/DNA (DAPI; blue). +GB indicates cultures treated with Golgi block (Brefeldin A). Ctrl refers to negative control. Data are representative of three independent experiments. Bars, 20 µm. (b) ATX protein levels in culture supernatants from WT and $hTNF^{+/-}$ SFs were analyzed by Western blot. 4F1 refers to a rat monoclonal Ab against ATX; Caym. refers to a commercial (Cayman Chemical) polyclonal Ab. Data are representative of four independent experiments. (c) Densitometric analysis of b. (d) Expression of ATX, vimentin, and VCAM by arthritic SFs was analyzed by flow cytometry. Data are representative of three independent experiments. (e) ATX mRNA in mouse WT SFs cultured for 24 h in the absence (control) or presence of 10 ng/ml TNF was analyzed by Q-RT-PCR ($n = 4$). Data are representative of three independent experiments. (c and e) Mean ± SE is shown. *, $P < 0.05$. (f and g) WT SFs were stimulated with the indicated concentrations of TNF, and cell extracts (f) or supernatants (g) were analyzed for ATX or tubulin expression by Western blot. Total protein in supernatants was quantified by the Bradford assay. Recombinant ATX (rATX) or native (nATX) was used as a positive control. Data are representative of two independent experiments. Black lines indicate that intervening lanes have been spliced out.

Published April 9, 2012

Anti-TNF treatment (biweekly intraperitoneal injections of 10 mg/kg infliximab) of the inflammatory animal model ($hTNF^{+/-}$) attenuated ATX expression (Fig. S1, e and f), consistent with the in vitro results, suggesting that ATX induction in arthritic SFs is a downstream event of exacerbated TNF signaling in the synovium.

The increased ATX expression from arthritic SFs was also verified at the transcriptional level by crossing arthritic ($hTNF^{+/-}$) mice with the heterozygous complete KO mouse for ATX ($Enpp2^{LacZ/+}$; Fig. 2 d), where the ATX promoter in one allele is driving LacZ expression instead of ATX (Koike et al., 2009). The results, in accordance with ATX immunostaining, indicate constitutive expression of ATX from chondrocytes in healthy tissue, exhibiting no appreciable expression differences upon disease development. On the contrary, low constitutive expression from SFs in healthy tissue was noted and found dramatically increased in the arthritic joint (Fig. 2 d). Increased ATX protein levels were also detected in the plasma of arthritic ($hTNF^{+/-}$) mice using ELISA assays (Fig. 2 e). Arthritic mice presented with decreased levels of LPC, the substrate of ATX, as measured by liquid chromatography mass spectrometry (LC/MS; Fig. 2 f); however, as other phospholipid enzymes are also involved in LPC metabolism, the decrease in LPC levels cannot be attributed solely to ATX. No differences were detected in LPA levels in both plasma and joint tissues (not depicted), most likely because of the rapid turnover of LPA (Albers et al., 2010) and the possible local delivery to its receptors by cell-bound ATX (Hausmann et al., 2011).

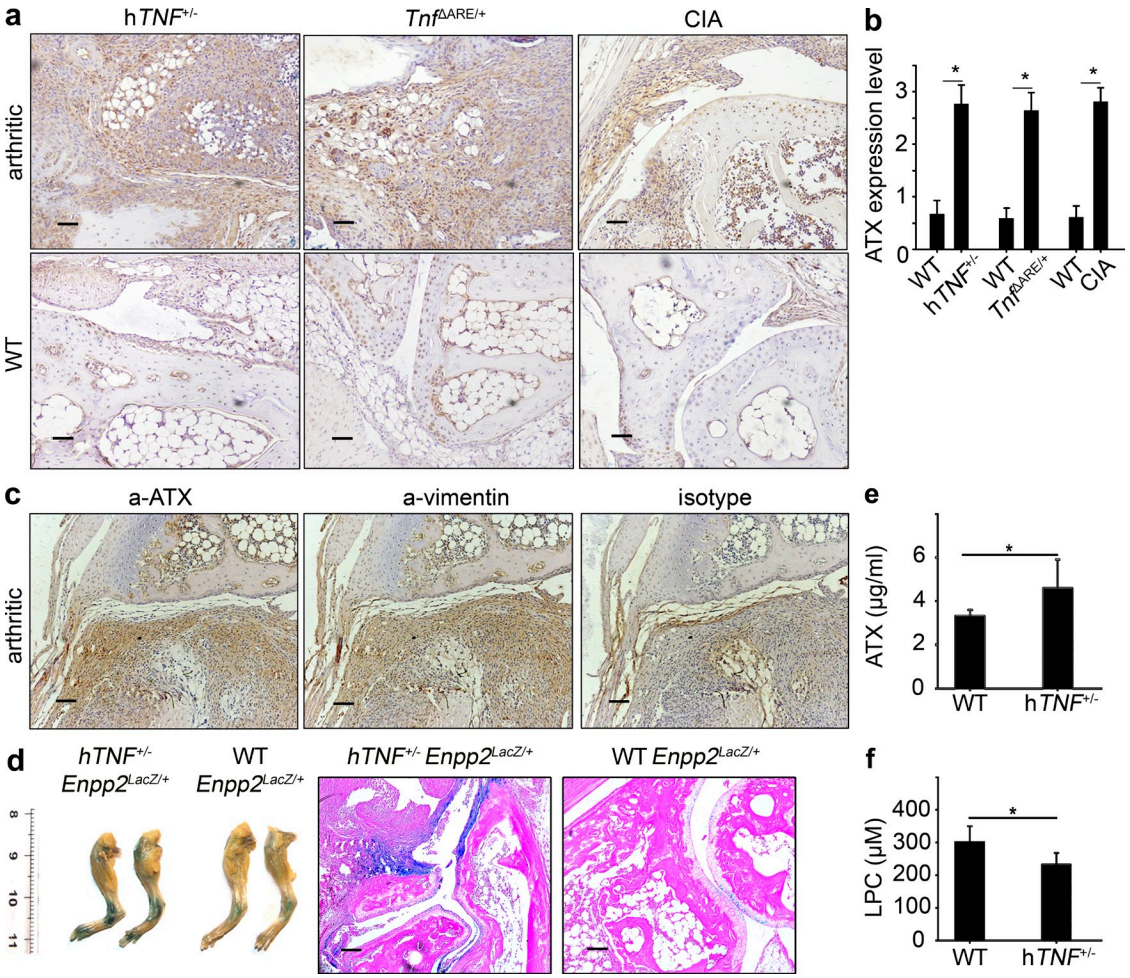

Figure 2. Increased ATX expression in mouse arthritic joints in vivo. (a) Representative immunohistochemistry images showing the expression of ATX in inflamed joints of three animal models of arthritis and respective WT littermate controls. Identical ATX staining was obtained in sequential sections (Fig. S1 a) and with different anti-ATX Abs (Fig. S1, b and c). (b) Quantification of ATX expression in mouse synovial tissues, as seen in a, was performed as described in Materials and methods ($hTNF^{+/-}$, $n = 10$; $Tnf^{\Delta ARE/+}$ and CIA, $n = 3$). (c) Immunostaining of ATX (and its isotype control) or vimentin in sequential sections of mouse synovial tissues. (d) Representative whole mount X-gal staining (left) and X-gal staining on joint sections (right) from WT and $hTNF^{+/-}$ mice carrying one genetically modified allele driving LacZ expression under the control of the ATX promoter ($n = 3$). (e) Plasma levels of ATX in littermate pairs of WT and $hTNF^{+/-}$ mice at the time of sacrifice ($n = 10$; litters = 4). (f) Measurement of (total) LPC plasma levels with LC/MS in WT and $hTNF^{+/-}$ mice at the time of sacrifice ($n = 9$; litters = 2). (b, e, and f) Mean ± SE is shown. *, $P < 0.05$. Bars, 50 µm.

Published April 9, 2012

Increased ATX expression from SFs of RA patients

Significant expression of ATX was also detected at the sublining areas and sites of destruction in joints of RA patients (Fig. 3, a–c), localized at SFs, as shown with double labeling with the fibroblast-specific marker collagen prolyl 4-hydroxylase (P4H; Fig. 3 d; Petrow et al., 2000). Moreover, SFs isolated from RA patients were shown to express significantly more ATX mRNA than SFs isolated from osteoarthritis (OA) patients (Fig. 3 e). ATX staining was also observed in T cell follicles of the arthritic synovium (not depicted), in line with the suggested function of ATX as an adhesive substrate for migrating lymphocytes (Kanda et al., 2008).

Increased ATX levels were also detected in the serum and synovial fluid of human RA patients (Fig. 3, f and g, respectively; no significant differences in age and sex distribution among groups). Consistent with results obtained from arthritic mice, decreased levels of LPC were found in the plasma of RA patients, in agreement with a previous study suggesting a role for phospholipid homeostasis in RA (Fig. 3 h; Fuchs et al., 2005). No significant differences in LPA levels were detected (not depicted). However, large cohort studies are required to establish ATX as a possible biomarker for RA and to examine phospholipid homeostasis in detail.

Conditional genetic ablation of ATX in mesenchymal cells attenuates disease development

To dissect the possible role of ATX in disease development, ATX expression was conditionally ablated using a conditional (LoxP) KO mouse for ATX (*Enpp2*$^{n/n}$; Fotopoulou et al., 2010) crossed with a transgenic mouse expressing the Cre recombinase under the control of the collagen VI (ColVI) promoter, resulting in 80% recombination efficiency in SFs (Armaka et al., 2008). No apparent phenotype was observed in *Enpp2*$^{-/-}$*ColVICre*$^{+/-}$ mice, which were healthy and fertile, exhibiting no differences in systemic levels of ATX/LPA (not depicted) and normal joint architecture (Fig. 4 c).

Arthritic disease development upon conditional deletion in SFs (and other mesenchymal cells) was first assessed in the inflammatory arthritis model (*hTNF*$^{+/-}$). The lack of ATX SF expression in the joints of *Enpp2*$^{-/-}$*ColVICre*$^{+/-}$*hTNF*$^{+/-}$ mice resulted in a striking decrease in inflammation and synovial hyperplasia, as indicated by histopathological analysis of the joints (Fig. 4, a and b). PCR analysis of DNA extracted from the corresponding joint sections indicated correct *Enpp2* recombination (Fig. S2 a). Ablation efficiency was further evaluated by immunohistochemical staining (Fig. S2 b), and a direct correlation of ATX expression with histopathological score was observed (Fig. S2 c). No decrease of the minimal constitutive ATX

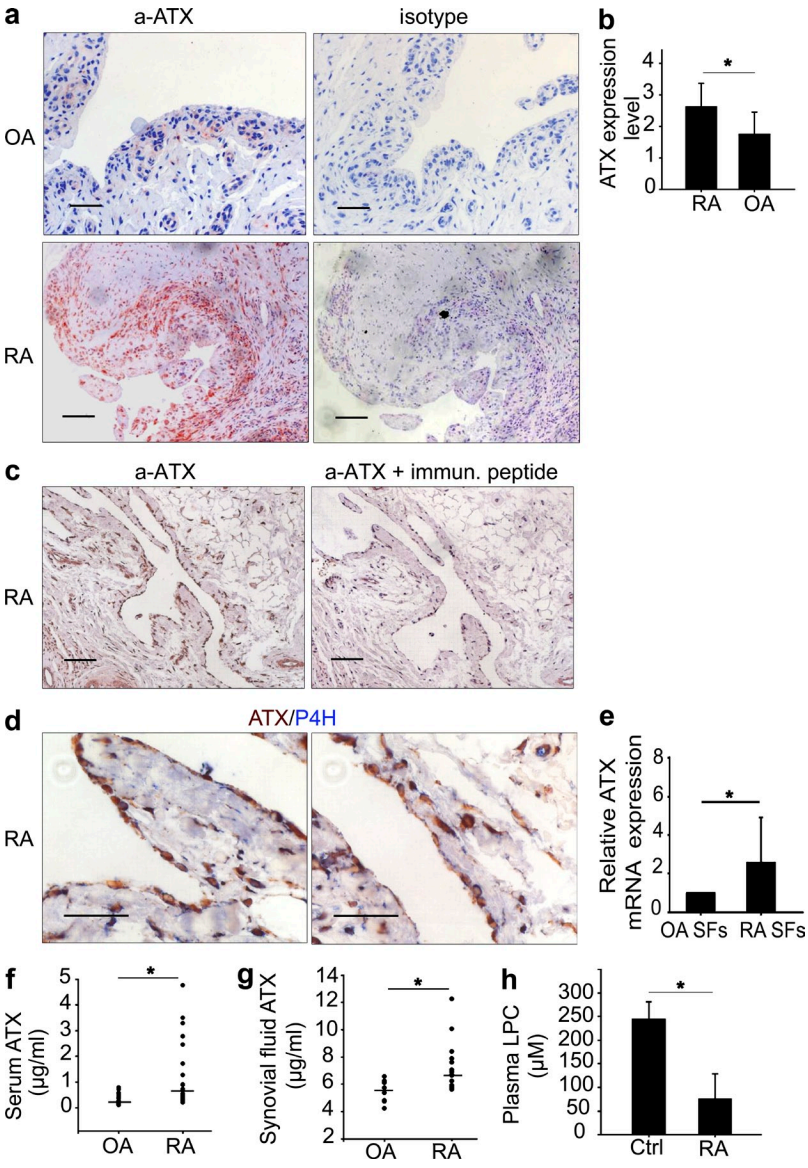

Figure 3. Increased ATX expression in RA patients. (a) Representative sections from RA and OA synovial tissues stained for ATX or isotype IgG control. (b) The expression of ATX from tissues shown in a was quantified as described in Materials and methods ($n = 8$). (c) ATX staining upon the addition of the immunogenic blocking peptide. (d) Representative double staining of human RA tissue section for ATX and P4H. (e) Real-time PCR analysis of ATX expression in SFs isolated from subjects with OA or RA ($n = 3$). (f) Measurement of ATX levels in sera from RA and OA patients ($n = 26$). Personal and clinical patient information is included in Table S1. (g) Measurement of synovial fluid ATX levels with ELISA from RA and OA patients ($n = 16$ and 9, respectively). (f and g) Values are expressed as medians, and statistical significance was assessed using the Mann-Whitney Rank Sum test. Asterisks indicate a statistically significant (*, $P < 0.05$) increase. (h) Measurement of (total) LPC plasma levels with LC/MS in RA patients and healthy controls (Ctrl; $n = 5$). (b, e, and h) Mean ± SE is shown. *, $P < 0.05$. Bars, 50 µm.

Published April 9, 2012

expression from articular chondrocytes was observed (not depicted), ruling out a direct involvement of ATX expression from this cell type in disease development.

To examine whether deletion of ATX in cells other than SFs could indirectly affect disease development by possibly modulating systemic plasma ATX levels, it was next investigated whether systemic fluctuations of ATX and LPA plasma levels are able to alter disease development. The arthritic *hTNF*$^{+/-}$ transgenic mice were mated with homozygous transgenic mice overexpressing ATX in the liver, driven by the human α1-antitrypsin inhibitor (*a1t1*) promoter (200% of normal plasma ATX and LPA levels; Pamuklar et al., 2009), as well as with the complete heterozygous KO mouse for ATX (50% of normal plasma ATX and LPA levels; Fotopoulou et al., 2010). No differences in the severity of arthritis were observed in this (*hTNF*$^{+/-}$) animal model (Fig. S3), highlighting the pathological role of the local, SF-specific ATX expression in disease development.

To confirm the role of ATX in disease development in an inducible, autoimmune model, the effect of SF-specific ATX genetic ablation in the development of CIA (Campbell et al., 2000) was next investigated. As expected for the C57BL/6 genetic background (Campbell et al., 2000), 50% of WT *Enpp2*$^{+/+}$*ColVICre*$^{+/-}$ mice developed disease symptoms, whereas the *Enpp2*$^{-/-}$*ColVICre*$^{+/-}$ littermate mice were found protected from disease development (Fig. S2, d and e). Histopathological analysis of joints (Fig. 4, c and d; and Fig. S2, f–h) revealed a lack of synovial inflammation upon ATX ablation in SFs, thus confirming the significant role of ATX in disease pathogenesis.

ATX stimulates SF activation and effector functions through LPA signaling

To dissect the mechanistic implications of increased ATX expression in synovial inflammation and arthritis pathogenesis, a series of in vitro experiments were performed. Primary mouse SFs were found to express all five major LPARs (not depicted), as has been previously shown for human SFs (Zhao et al., 2008). Addition of LPA, but not LPC (if ATX was not added to convert it to LPA), to primary cultures stimulated the proliferation of WT SFs in a dose-dependent manner (Fig. 5, a–c) but did not affect macrophages that also express all major LPARs (not depicted). On the contrary, LPC was able to stimulate the proliferation of arthritic SFs, most likely because of their increased production of active ATX (Fig. 5 b). LPA stimulation of SFs also resulted in their increased adhesion and migration (Fig. 5, d and e, respectively), accompanied by rearrangements of their actin cytoskeleton (Fig. 5 f), as well as in the production of MMP9 (matrix metalloproteinase 9; Q-RT-PCR; Fig. 5 g), all previously reported to be functional properties of arthritic SFs (Aidinis et al., 2005). In addition, multiplex Luminex bead assays showed that LPA stimulated the secretion of various proinflammatory cytokines from SFs (TNF, IL-6, KC, MIP-1a, and RANTES; Fig. 5 h) but not from bone marrow–derived macrophages, activated or not (not depicted). More importantly, LPA was shown to synergize with TNF (Fig. 5 i), as previously reported for PDGF and EGF in other cell types (Cerutis et al., 1997; Sakai et al., 1999), suggesting that the ATX/LPA axis is important in regulating and/or amplifying growth factor responses. LPA responses were inhibited not only by an inhibitor of G-protein signaling as expected (PTX; Fig. 5 j), but also by inhibitors of ERK (extracellular signal-regulated kinase), p38, JNK, and Rho kinase signaling (PD98059, SB203580, SP600125, and Y27632, respectively; Fig. 5 j). Therefore, LPA stimulates its G-protein–coupled receptors, leading to mitogen-activated protein kinase (GPCR/MAPK)–dependent activation of SFs and their effector functions, consistent with its reported functions in various fibroblasts in different tissues (Nochi et al., 2008).

In conclusion, this study suggests that the proinflammatory milieu during the pathogenesis of RA stimulates local, TNF-driven, SF-specific ATX expression in the synovium, leading to

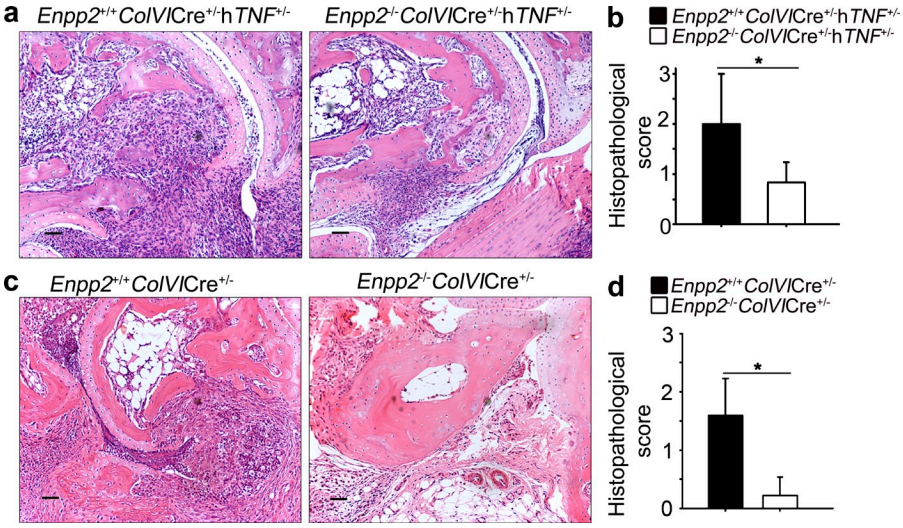

Figure 4. Genetic ablation of ATX from mesenchymal cells attenuates disease development. (a) Representative H&E-stained sections of ankle joints from *hTNF*$^{+/-}$ mice with (*Enpp2*$^{-/-}$*ColVICre*$^{+/-}$) or without (*Enpp2*$^{+/+}$*ColVICre*$^{+/-}$) genetic deletion of ATX from SFs. (b) Quantification of disease severity in *Enpp2*$^{-/-}$*ColVICre*$^{+/-}$*hTNF*$^{+/-}$ and *Enpp2*$^{+/+}$*ColVICre*$^{+/-}$*hTNF*$^{+/-}$ mice (n = 7; litters = 2). (c) Representative H&E-stained joint sections of *Enpp2*$^{-/-}$*ColVICre*$^{+/-}$ and *Enpp2*$^{+/+}$*ColVICre*$^{+/-}$ mice upon CIA induction. (d) Quantitative assessment of synovial inflammation in *Enpp2*$^{-/-}$*ColVICre*$^{+/-}$ and *Enpp2*$^{+/+}$*ColVICre*$^{+/-}$ mice (n = 7; litters = 2). (b and d) Mean ± SE is shown. *, $P < 0.05$. Bars, 50 µm.

Published April 9, 2012

the hydrolysis of circulating LPC and the local production of LPA. In turn, LPA activates SFs and their effector functions and amplifies and/or regulates pathogenetic responses in synergy with TNF. Genetic deletion of ATX from SFs resulted in disease attenuation in animal models of arthritis, thus establishing ATX as a novel player in chronic inflammation and the pathogenesis of arthritis and a promising therapeutic target.

MATERIALS AND METHODS

Animals. All mice were bred at the animal facilities of the Alexander Fleming Biomedical Sciences Research Center (BSRC) under specific pathogen–free conditions. Mice were housed at a temperature of 20–22°C, 55 ± 5% humidity, and a 12-h light–dark cycle; water and food were given ad libitum. Mice were bred and maintained in their respective genetic backgrounds for >10 generations. All experiments were approved by the Institutional Animal Ethic Committee of BSRC Fleming (#232), as well as by the Veterinary Service and Fishery Department of the local government agency.

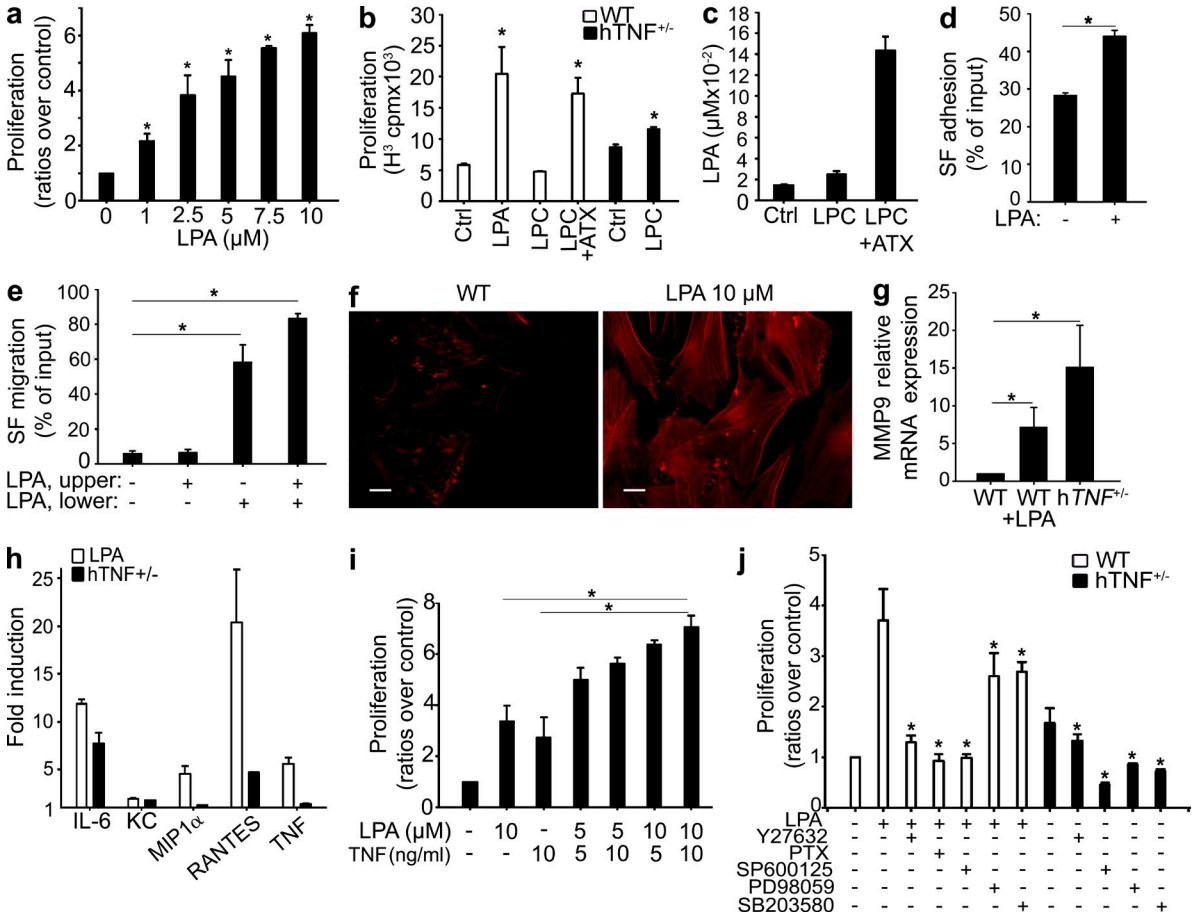

Figure 5. ATX stimulates SF activation and effector functions through LPA signaling. (a) Mouse WT SFs were stimulated for 24 h with the indicated concentrations of LPA, and proliferation was measured with a [^{3}H]thymidine uptake assay. Data are representative of eight independent experiments. All values were normalized and compared with control values. (b) Mouse WT and *hTNF*$^{+/-}$ SFs were stimulated for 24 h with 10 μM LPA, 10 μM LPC, or 10 μM LPC together with 4 nM ATX, and proliferation was measured as in a (n = 3). Data are representative of three independent experiments. (c) LPA levels in culture supernatants from b. (d) SFs were plated in fibronectin-coated wells in the presence or absence of 10 μM LPA, and their adhesion was measured as described in Materials and methods. Data are representative of three independent experiments. (e) SFs were plated on Boyden chambers and were allowed to migrate under the influence of LPA for 4 h. Data are representative of three experiments. (f) SFs were treated for 4 h at 37°C with 10 μM LPA, and F-actin was stained with TRITC–conjugated phalloidin. Data are representative of five independent experiments. Bars, 20 μm. (g) Mouse WT and *hTNF*$^{+/-}$ SFs were cultured for 4 h in the presence or absence of 10 μM LPA, and MMP9 mRNA was assessed with Q-RT–PCR. Results were normalized to the expression of b2m. Data are representative of three independent experiments. (h) Proinflammatory cytokine levels measured by ELISA in culture supernatants from mouse WT or *hTNF*$^{+/-}$ SFs, stimulated or not for 4 h with 10 μM LPA. Values were expressed as ratios over control (WT SFs). Data are representative of three independent experiments. (i) Mouse WT SFs were stimulated for 24 h with the indicated concentrations of LPA and/or TNF, and proliferation was measured as in a. All values were normalized to control values. The asterisks indicate a statistically significant (*, $P < 0.001$) increase of the combined TNF/LPA treatment as compared with individual treatments. Differences between all experimental group values were also statistically significant compared with control. Data are representative of three experiments. Mean ± SE is shown. (j) Mouse WT and *hTNF*$^{+/-}$ SFs were treated with 10 μM LPA, a G-protein inhibitor (50 ng/ml PTX), a Rho kinase inhibitor (10 μM Y27632), or JNK, ERK, and p38 inhibitors (10 μM SP600125, 10 μM PD98059, and 5 μM SB203580, respectively), and proliferation was measured as in a. Data are representative of three independent experiments. (a–e, g, h, and j) Mean ± SE is shown. *, $P < 0.05$.

Published April 9, 2012

The generation and genotyping instructions of *Tg197* (*hTNF*$^{+/-}$; Keffer et al., 1991), *Tnf*$^{\Delta ARE}$ (Kontoyiannis et al., 1999), *ColVI-Cre* (Armaka et al., 2008), *Enpp2*$^{LacZ/n}$ (Koike et al., 2009), *Enpp2*$^{n/n}$ (Fotopoulou et al., 2010), and Tg(*a1t1*)*ATX*$^{+/+}$ (Pamuklar et al., 2009) mice have been previously described.

Animal models of arthritis. Both inducible and spontaneous animal models of arthritis were used in this study (Kollias et al., 2011). CIA was induced in C57BL/6 mice as previously described (Campbell et al., 2000). In brief, mice were immunized with chicken collagen type II, followed by a boost immunization at day 21. Disease onset was observed at day 28; all experimental mice were sacrificed at day 60 after immunization. *Tg197* (*hTNF*$^{+/-}$) is a humanized TNF transgenic mouse with human TNF overexpression resulting in the spontaneous development of chronic, erosive, and symmetrical polyarthritis (Kollias et al., 2011). Disease symptoms were observed 3 wk after birth; all experimental mice were sacrificed 5–6 wk after birth. *Tnf*$^{\Delta ARE}$ is a mouse mutant carrying a deletion of the ARE (AU-rich elements), 3′ untranslated region regulatory element of TNF that results in loss of its posttranscriptional regulation. Deregulated TNF expression leads to the gradual development of spontaneous inflammatory polyarthritis and inflammatory bowel disease (Kontoyiannis et al., 1999).

Patients. Human synovial tissues and SFs were obtained at the time of joint replacement surgery at the Schulthess Clinic (Zurich, Switzerland). Sera from patients were obtained from the Schulthess Clinic. All patients, classified according to the 1987 criteria of the American College of Rheumatology, signed an informed consent form where they agreed to the anonymous use of their samples for research purposes after approval of the Kantonale Ethikkommission, Spezialisierte Unterkommission für Spezialfächer (#475). All personal and clinical data of patients are included in Tables S1 and S2.

Reagents. 1-oleoyl-LPA (18:1) and 1-oleoyl-LPC (18:1) were purchased from Avanti Polar Lipids, Inc. ERK inhibitor PD98059, p38 MAPK inhibitor SB202190, and JNK inhibitor SP600125 were obtained from EMD. Fatty acid–free BSA, choline oxidase, peroxidase, TMB (3,3′,5,5′-tetramethylbenzidine) substrate, phalloidin, and DAB (3,3′-diaminobenzidine) were obtained from Sigma-Aldrich. Recombinant ATX and mouse TNF were purchased from R&D Systems. Native ATX refers to the 10× concentrated supernatants of MDA-MB-43S cells (American Type Culture Collection), which are highly enriched in ATX. Fibronectin and Cytofix/Cytoperm solution were obtained from BD. Rabbit anti-ATX polyclonal antibodies (Abs) were purchased from Phoenix Pharmaceuticals and/or Cayman Chemical; rat monoclonal Abs (clone 4F1) against ATX were a gift from J. Aoki (Tohoku University, Aoba-ku, Sendai, Miyagi, Japan). Antivimentin Abs were purchased from Millipore, and collagen P4H Abs were purchased from Acris. Secondary Alexa Fluor 555–conjugated anti–rabbit Ab was obtained from Invitrogen; all secondary horseradish peroxidase (HRP)–conjugated Abs and isotype controls were obtained from and SouthernBiotech.

Histopathology and arthritic score. Paraffin-embedded mouse joint tissue samples were sectioned and stained with hematoxylin and eosin (H&E) as previously described (Aidinis et al., 2005; Armaka et al., 2008). Arthritic histopathology in mice was assessed (in a blinded fashion from three independent reviewers) using a semiquantitative scoring system as previously described for CIA (0 = no detectable pathology; 1 = mild arthritis, minimal synovitis and cartilage loss; 2 = moderate arthritis, synovitis and bone erosions; and 3 = severe arthritis, synovitis, extensive erosions, and disrupted joint architecture; Campbell et al., 2000). The scoring system for *Tg197* (*hTNF*$^{+/-}$) is as follows: 0 = no detectable pathology, 1 = synovial membrane hyperplasia, 2 = pannus and fibrous tissue formation and focal bone erosion, 3 =cartilage destruction and bone erosion, and 4 = extensive cartilage destruction and bone erosion.

Immunohistochemistry. Paraffin-embedded mouse joint tissue samples (4-µm-thick sections) were deparaffinized, and endogenous peroxidase activity was blocked by incubation in 1% H_2O_2 for 10 min. Sections were then blocked with 2% BSA for 30 min and incubated overnight at 4°C with an anti-ATX Ab (from Phoenix Pharmaceuticals unless otherwise indicated) or an IgG rabbit isotype control. Washing in PBS-T was followed by incubation with HRP-conjugated anti–rabbit IgG for 30 min at room temperature. Bound peroxidase activity was detected by staining with DAB. Sections were counterstained with hematoxylin, mounted, and photographed under an ECLIPSE E800 microscope (Nikon) using the ACT-I software. Expression levels were quantified by using a three-point scale semiquantitative intensity score: 0 = no staining, 1 = weak expression, 2 = moderate expression, and 3 = strong expression.

Formalin-fixed, paraffin-embedded sections of RA and OA synovial tissue slides were deparaffinized and treated at 80°C for 30 min with citrate buffer, pH 6.0. After washing with H_2O, the endogenous peroxidase was blocked with 1% H_2O_2 for 10 min. The slides were blocked with 2% goat serum for 1 h and incubated overnight at 4°C with a rabbit polyclonal Ab against ATX (Cayman Chemical) or IgG1 rabbit isotype control (Dako). After washing twice in PBS, the slides were incubated with their respective biotinylated secondary Abs for 30 min. The signal was amplified with HRP conjugated with streptavidin Vectastain Elite ABC kit (Vector Laboratories). The slides were then developed with a chromogenic substrate for peroxidase and counterstained with hematoxylin. ATX expression was quantified semiquantitatively, blindly by three different reviewers, on a five-point scale: 0 = no staining; 1 = weak expression, single cells stained; 2 = mild expression, limited areas stained; 3 = moderate expression, weak overall expression; and 4 = strong expression, strong overall staining.

LacZ staining. Joints were harvested as a block, and a paramedical patella incision was made on the joint to expose the inside. Harvested joints were fixed in formaldehyde/glutaraldehyde for 1 h at room temperature, washed three times in PBS/2 mM $MgCl_2$, and incubated with 1 mg/ml 5-bromo-a-chloro-3-inodyl-β-D-galactopyranoside (X-gal) in 0.1 M Na phosphate buffer, pH 7.3 (2 mM $MgCl_2$, 0.01% Na deoxycholate, 0.02% NP-40, 5 mM $K_3Fe(CN)_6$, and 5 mM $K_4Fe(CN)_6$) at 37°C in the dark overnight. Tissues were rinsed three times in PBS/2 mM $MgCl_2$ at room temperature and were then placed in decalcification buffer at 4°C for 6 d. After that, they were washed with PBS and embedded in paraffin. The resulting 4-µm sections were counterstained with eosin and visualized under an ECLIPSE E800 microscope as in the previous section.

Cell isolation and culture. Primary SFs were isolated by enzymatic treatment of the joints of 6-wk-old mice as previously described (Aidinis et al., 2005). Cells from two to three mice were pooled and cultured in standard conditions: DME supplemented with 10% FBS and 1% penicillin-streptomycin, 37°C, and 5% CO_2 (Aidinis et al., 2005); all experiments were performed after two to three passages with 70–80% confluent cells and confirmed with independent isolations. All in vitro experiments were performed after overnight serum starvation (supplemented with 0.2% fatty acid–free BSA). Cells were pretreated with the indicated concentrations of PTX and inhibitors of ERK, p38, JNK, and Rho kinase for 3 h before LPA stimulation. Brefeldin A (GolgiPlug; BD) was added to SF cultures for 4 h according to manufacturer's instructions to prevent Golgi transport.

Flow cytometry. Cells were initially stained extracellularly with VCAM-1 (CD106) and subsequently with a secondary (PE) conjugated Ab. For intracellular stainings, cells were fixed and permeabilized with Cytofix/Cytoperm solution, followed by incubation with anti-ATX (1:200; Cayman Chemical) and antivimentin (1:50) Abs for 30 min. Primary Abs were detected after a 30-min incubation with anti–rabbit biotin Abs followed by PE-Cy5-streptavidin or with FITC-conjugated secondary Ab (all diluted 1:500). Analysis was performed using FACSCanto II and Diva software (BD).

Proliferation assay. SFs were grown in 24-well tissue-culture plates in DME. Preconfluent cell cultures were starved overnight, incubated for 24 h with LPA and the various compounds, and finally exposed to 0.5 µCi/ml

Published April 9, 2012

[^{3}H]thymidine. Cells were then washed with PBS, detached with 0.05% trypsin, and blotted on FilterMAT fiber paper using a cell harvester (Molecular Devices). The radioactivity of incorporated [^{3}H]thymidine was determined using a liquid scintillation counter (LS 6500; Beckman Coulter). The experiments were performed in triplicate.

Adhesion assay. This assay was performed on plates coated with human fibronectin (10 µg/ml in PBS) for 2 h at 37°C. In brief, cells were allowed to adhere to the substrate for 4 h at 37°C, and unbound cells were removed by washing twice with PBS. Adhered cells were then stained with 0.2% crystal violet in 10% ethanol for 10 min at room temperature. After washing with water, cells were lysed with 33% acetic acid, and their absorbance was determined at 570 nm using a SpectraMax Plus photometer (Molecular Devices). The experiments were performed in triplicate.

Cell migration assay. Modified Boyden chambers with 8-µm pores (Corning) were coated at the lower surface with 10 µg/ml human fibronectin for 2 h at 37°C. Cells were harvested with trypsin/EDTA from nonconfluent cultures, washed with PBS, and resuspended to 10^6 cells per ml. The cell suspension was then added to the upper chamber, and the cells were allowed to migrate at 37°C, 5% CO_2, for 4 h. Nonmigratory cells were removed from the upper surface of the membrane, whereas migratory cells in the lower compartment of the chambers were washed with PBS and stained with 0.2% crystal violet in 10% ethanol for 10 min. After extensive washing in H_2O, the cells were lysed, and absorbance was measured at 570 nm with a SpectraMax Plus photometer as in the previous section. The experiments were performed in triplicate.

Immunofluorescence. Cells were cultured on glass coverslips, in the presence or absence of Brefeldin A, fixed in 4% paraformaldehyde, and stained with a primary Ab (1:300) against ATX (Cayman Chemical) overnight at 4°C. After incubation with a secondary anti–rabbit Ab (1:1,000) conjugated to Alexa Fluor 555 for 1 h at room temperature, cells were observed and photographed with an ECLIPSE E800 microscope as in Immunohistochemistry. F-actin (Sigma-Aldrich) was visualized with incubation with TRITC-conjugated phalloidin according to the manufacturer's protocol, after permeabilization with 0.1% Triton X-100 in PBS.

SDS-PAGE/Western blotting. The protein concentration of cell extracts or supernatants was determined with a Protein Assay kit (Bio-Rad Laboratories) using BSA as a standard. Supernatants or cellular extracts from cultured SFs were separated by 8% SDS-PAGE and transferred to Protran nitrocellulose membranes (GE Healthcare) using the Trans-Blot SD Semi-Dry Transfer system (Bio-Rad Laboratories). Primary anti-ATX Ab incubation (monoclonal 4F1, 1:1,000, unless otherwise specified) was performed overnight in 2.5% (wt/vol) nonfat milk at 4°C. The membranes were then washed three times with TBS-Tween 0.05% and incubated with an anti–rat HRP-conjugated secondary Ab (1:1,000) for 1 h at room temperature. Membranes were washed three times with TBS-Tween 0.05%, and Ab–antigen complexes were revealed using luminol as a chemiluminescent reagent.

ELISAs. Plates were coated overnight with standards and diluted samples, blocked with 2% BSA, and then incubated with an anti-ATX Ab (Cayman Chemical). For mouse plasma, dilution was 1:16, for human serum 1:40, and for human synovial fluids 1:120, selected from the linear range of serial dilutions. ATX antigen was detected after incubation with an HRP-labeled secondary Ab and development with TMB substrate. Readings were obtained at 450 nm with a SpectraMax Plus photometer. Cytokine levels in mouse cell culture supernatants were determined using the multiplex LINCOplex assay kit (Millipore), according to the manufacturer's instructions.

RNA extraction and RT-PCR analysis. RNA extraction and RT-PCR analysis were performed as previously described (Aidinis et al., 2005). Immune cell RNAs were provided by P. Stamou and D.L. Kontoyiannis (Alexander Fleming Biomedical Sciences Research Center, Athens, Greece). Primer sequences (designated as s, sense; and as, antisense) and product sizes were as follows: Enpp2 (s, 5′-GTGAAATATTCTTAATGCCTCTCTG-3′; as, 5′-GCCTTCCACATACTGTTTAATTCC-3′; 410 bp), b2m (s, 5′-TTCTGGTGCTTGTCTCACTGA-3′; as, 5′-CAGTATGTTCGGCTTCCCATTC-3′; 104 bp), MMP-9 (s, 5′-CAGATGATGGGAGAGAAGCA-3′; as, 5′-CGGCAAGTCTTCAGAGTAGT-3′; 222 bp), LPA1 (s, 5′-GAGGAATCGGGACA-3′; as, 5′-TGAAGGTGGCGCTC-3′; 227 bp), LPA2 (s, 5′-GACCACACTCAGCCTAGTCAAGAC-3′; as, 5′-CAGCATCTCGGCAGGAAT-3′; 200 bp), LPA3 (s, 5′-GCTCCCATGAAGCTAATGAAGACA-3′; as, 5′-TACGAGTAGATGATGGGG-3′; 188 bp), LPA4 (s, 5′-AGTGCCTCCCTGTTTGTCTTC-3′; as, 5′-GCCAGTGGCGATTAAAGTTGTAA-3′; 142 bp), and LPA5 (s, 5′-ACCCTGGAGGTGAAAGTC-3′; as, 5′-GACCACCATATGCAAACG-3′; 176 bp).

Statistical analysis. Unless otherwise indicated, statistical significance was assessed in pairwise comparisons with control values by using a paired Student's *t* test, after confirmation of normal distributions with SigmaPlot 11.0 (Systat Software). Unless otherwise indicated, all values are expressed as means ± SE, and p-values <0.05 were considered significant (*).

Online supplemental material. Fig. S1 contains various controls supporting an increased ATX expression in arthritic joints, as well as supporting that TNF treatment of the transgenic animal model of arthritis attenuates ATX expression. Fig. S2 contains various controls on the effects of the conditional ATX deletion in modeled disease development. Fig. S3 shows that systemic fluctuations of ATX serum levels do not affect disease development in the *hTNF*$^{+/-}$ animal model. Tables S1 and S2 contain personal and clinical data of patients used for determination of ATX levels in sera and synovial fluids, respectively. Online supplemental material is available at http://www.jem.org/cgi/content/full/jem.20112012/DC1.

We would like to thank V. Harokopos, A. Thanassopoulou, and S. Lalos for expert technical assistance, P. Stamou and D.L. Kontoyiannis for the immune cell RNAs, J. Aoki for monoclonal Abs against ATX, and M.N. Manoussakis and H. Moutsopoulos for valuable discussions and continuous support.

This work was supported by the following grants: European Commission LSHG-CT-2005-005203, European Commission HEALTH-F2-2008-223404, Innovative Medicines Initiative Joint Undertaking BTCure#115142, and the Hellenic Ministry for Development GSRT-PENED-136.

The authors have no conflicting financial interests.

Submitted: 20 September 2011
Accepted: 12 March 2012

REFERENCES

Aidinis, V., P. Carninci, M. Armaka, W. Witke, V. Harokopos, N. Pavelka, D. Koczan, C. Argyropoulos, M.M. Thwin, S. Möller, et al. 2005. Cytoskeletal rearrangements in synovial fibroblasts as a novel pathophysiological determinant of modeled rheumatoid arthritis. *PLoS Genet.* 1:e48. (published erratum appears in *PLoS Genet.* 2005. 1:e73) http://dx.doi.org/10.1371/journal.pgen.0010048

Albers, H.M., A. Dong, L.A. van Meeteren, D.A. Egan, M. Sunkara, E.W. van Tilburg, K. Schuurman, O. van Tellingen, A.J. Morris, S.S. Smyth, et al. 2010. Boronic acid-based inhibitor of autotaxin reveals rapid turnover of LPA in the circulation. *Proc. Natl. Acad. Sci. USA.* 107:7257–7262. http://dx.doi.org/10.1073/pnas.1001529107

Aoki, J. 2004. Mechanisms of lysophosphatidic acid production. *Semin. Cell Dev. Biol.* 15:477–489. http://dx.doi.org/10.1016/j.semcdb.2004.05.001

Armaka, M., M. Apostolaki, P. Jacques, D.L. Kontoyiannis, D. Elewaut, and G. Kollias. 2008. Mesenchymal cell targeting by TNF as a common pathogenic principle in chronic inflammatory joint and intestinal diseases. *J. Exp. Med.* 205:331–337. http://dx.doi.org/10.1084/jem.20070906

Bächner, D., M. Ahrens, D. Schröder, A. Hoffmann, J. Lauber, N. Betat, P. Steinert, L. Flohé, and G. Gross. 1998. Bmp-2 downstream targets in mesenchymal development identified by subtractive cloning from recombinant mesenchymal progenitors (C3H10T1/2). *Dev. Dyn.* 213:398–411.

Published April 9, 2012

http://dx.doi.org/10.1002/(SICI)1097-0177(199812)213:4<398::AID-AJA5>3.0.CO;2-T

Campbell, I.K., J.A. Hamilton, and I.P. Wicks. 2000. Collagen-induced arthritis in C57BL/6 (H-2b) mice: new insights into an important disease model of rheumatoid arthritis. *Eur. J. Immunol.* 30:1568–1575. http://dx.doi.org/10.1002/1521-4141(200006)30:6<1568::AID-IMMU1568>3.0.CO;2-R

Cerutis, D.R., M. Nogami, J.L. Anderson, J.D. Churchill, D.J. Romberger, S.I. Rennard, and M.L. Toews. 1997. Lysophosphatidic acid and EGF stimulate mitogenesis in human airway smooth muscle cells. *Am. J. Physiol.* 273:L10–L15.

Choi, J.W., C.W. Lee, and J. Chun. 2008. Biological roles of lysophospholipid receptors revealed by genetic null mice: an update. *Biochim. Biophys. Acta.* 1781:531–539.

Edwards, J.C. 2000. Fibroblast biology. Development and differentiation of synovial fibroblasts in arthritis. *Arthritis Res.* 2:344–347. http://dx.doi.org/10.1186/ar110

Fotopoulou, S., N. Oikonomou, E. Grigorieva, I. Nikitopoulou, T. Paparountas, A. Thanassopoulou, Z. Zhao, Y. Xu, D.L. Kontoyiannis, E. Remboutsika, and V. Aidinis. 2010. ATX expression and LPA signalling are vital for the development of the nervous system. *Dev. Biol.* 339:451–464. http://dx.doi.org/10.1016/j.ydbio.2010.01.007

Fuchs, B., J. Schiller, U. Wagner, H. Häntzschel, and K. Arnold. 2005. The phosphatidylcholine/lysophosphatidylcholine ratio in human plasma is an indicator of the severity of rheumatoid arthritis: investigations by 31P NMR and MALDI-TOF MS. *Clin. Biochem.* 38:925–933. http://dx.doi.org/10.1016/j.clinbiochem.2005.06.006

Hausmann, J., S. Kamtekar, E. Christodoulou, J.E. Day, T. Wu, Z. Fulkerson, H.M. Albers, L.A. van Meeteren, A.J. Houben, L. van Zeijl, et al. 2011. Structural basis of substrate discrimination and integrin binding by autotaxin. *Nat. Struct. Mol. Biol.* 18:198–204. http://dx.doi.org/10.1038/nsmb.1980

Kanda, H., R. Newton, R. Klein, Y. Morita, M.D. Gunn, and S.D. Rosen. 2008. Autotaxin, an ectoenzyme that produces lysophosphatidic acid, promotes the entry of lymphocytes into secondary lymphoid organs. *Nat. Immunol.* 9:415–423. http://dx.doi.org/10.1038/ni1573

Karouzakis, E., R.E. Gay, S. Gay, and M. Neidhart. 2009. Epigenetic control in rheumatoid arthritis synovial fibroblasts. *Nat. Rev. Rheumatol.* 5:266–272. http://dx.doi.org/10.1038/nrrheum.2009.55

Keffer, J., L. Probert, H. Cazlaris, S. Georgopoulos, E. Kaslaris, D. Kioussis, and G. Kollias. 1991. Transgenic mice expressing human tumour necrosis factor: a predictive genetic model of arthritis. *EMBO J.* 10:4025–4031.

Kehlen, A., R. Lauterbach, A.N. Santos, K. Thiele, U. Kabisch, E. Weber, D. Riemann, and J. Langner. 2001. IL-1 beta- and IL-4-induced down-regulation of autotaxin mRNA and PC-1 in fibroblast-like synoviocytes of patients with rheumatoid arthritis (RA). *Clin. Exp. Immunol.* 123:147–154. http://dx.doi.org/10.1046/j.1365-2249.2001.01432.x

Koike, S., K. Keino-Masu, T. Ohto, F. Sugiyama, S. Takahashi, and M. Masu. 2009. Autotaxin/lysophospholipase D-mediated lysophosphatidic acid signaling is required to form distinctive large lysosomes in the visceral endoderm cells of the mouse yolk sac. *J. Biol. Chem.* 284:33561–33570. http://dx.doi.org/10.1074/jbc.M109.012716

Kollias, G., P. Papadaki, F. Apparailly, M.J. Vervoordeldonk, R. Holmdahl, V. Baumans, C. Desaintes, J. Di Santo, J. Distler, P. Garside, et al. 2011. Animal models for arthritis: innovative tools for prevention and treatment. *Ann. Rheum. Dis.* 70:1357–1362. http://dx.doi.org/10.1136/ard.2010.148551

Kontoyiannis, D., M. Pasparakis, T.T. Pizarro, F. Cominelli, and G. Kollias. 1999. Impaired on/off regulation of TNF biosynthesis in mice lacking TNF AU-rich elements: implications for joint and gut-associated immunopathologies. *Immunity.* 10:387–398. http://dx.doi.org/10.1016/S1074-7613(00)80038-2

Mills, G.B., and W.H. Moolenaar. 2003. The emerging role of lysophosphatidic acid in cancer. *Nat. Rev. Cancer.* 3:582–591. http://dx.doi.org/10.1038/nrc1143

Müller-Ladner, U., T. Pap, R.E. Gay, M. Neidhart, and S. Gay. 2005. Mechanisms of disease: the molecular and cellular basis of joint destruction in rheumatoid arthritis. *Nat. Clin. Pract. Rheumatol.* 1:102–110. http://dx.doi.org/10.1038/ncprheum0047

Nochi, H., H. Tomura, M. Tobo, N. Tanaka, K. Sato, T. Shinozaki, T. Kobayashi, K. Takagishi, H. Ohta, F. Okajima, and K. Tamoto. 2008. Stimulatory role of lysophosphatidic acid in cyclooxygenase-2 induction by synovial fluid of patients with rheumatoid arthritis in fibroblast-like synovial cells. *J. Immunol.* 181:5111–5119.

Pamuklar, Z., L. Federico, S. Liu, M. Umezu-Goto, A. Dong, M. Panchatcharam, Z. Fulkerson, E. Berdyshev, V. Natarajan, X. Fang, et al. 2009. Autotaxin/lysopholipase D and lysophosphatidic acid regulate murine hemostasis and thrombosis. *J. Biol. Chem.* 284:7385–7394. (published erratum appears in *J. Biol. Chem.* 2009. 284:21100) http://dx.doi.org/10.1074/jbc.M807820200

Petrow, P.K., K.M. Hummel, J. Schedel, J.K. Franz, C.L. Klein, U. Müller-Ladner, J. Kriegsmann, P.L. Chang, C.W. Prince, R.E. Gay, and S. Gay. 2000. Expression of osteopontin messenger RNA and protein in rheumatoid arthritis: effects of osteopontin on the release of collagenase 1 from articular chondrocytes and synovial fibroblasts. *Arthritis Rheum.* 43:1597–1605. http://dx.doi.org/10.1002/1529-0131(200007)43:7<1597::AID-ANR25>3.0.CO;2-0

Sakai, T., J.M. de la Pena, and D.F. Mosher. 1999. Synergism among lysophosphatidic acid, beta1A integrins, and epidermal growth factor or platelet-derived growth factor in mediation of cell migration. *J. Biol. Chem.* 274:15480–15486. http://dx.doi.org/10.1074/jbc.274.22.15480

Santos, A.N., D. Riemann, A.N. Santos, A. Kehlen, K. Thiele, and J. Langner. 1996. Treatment of fibroblast-like synoviocytes with IFN-gamma results in the down-regulation of autotaxin mRNA. *Biochem. Biophys. Res. Commun.* 229:419–424. http://dx.doi.org/10.1006/bbrc.1996.1819

Stefan, C., S. Jansen, and M. Bollen. 2005. NPP-type ectophosphodiesterases: unity in diversity. *Trends Biochem. Sci.* 30:542–550. http://dx.doi.org/10.1016/j.tibs.2005.08.005

van Meeteren, L.A., and W.H. Moolenaar. 2007. Regulation and biological activities of the autotaxin-LPA axis. *Prog. Lipid Res.* 46:145–160. http://dx.doi.org/10.1016/j.plipres.2007.02.001

Zhao, C., M.J. Fernandes, G.D. Prestwich, M. Turgeon, J. Di Battista, T. Clair, P.E. Poubelle, and S.G. Bourgoin. 2008. Regulation of lysophosphatidic acid receptor expression and function in human synoviocytes: implications for rheumatoid arthritis? *Mol. Pharmacol.* 73:587–600. http://dx.doi.org/10.1124/mol.107.038216

SUPPLEMENTAL MATERIAL

Nikitopoulou et al., http://www.jem.org/cgi/content/full/jem.20112012/DC1

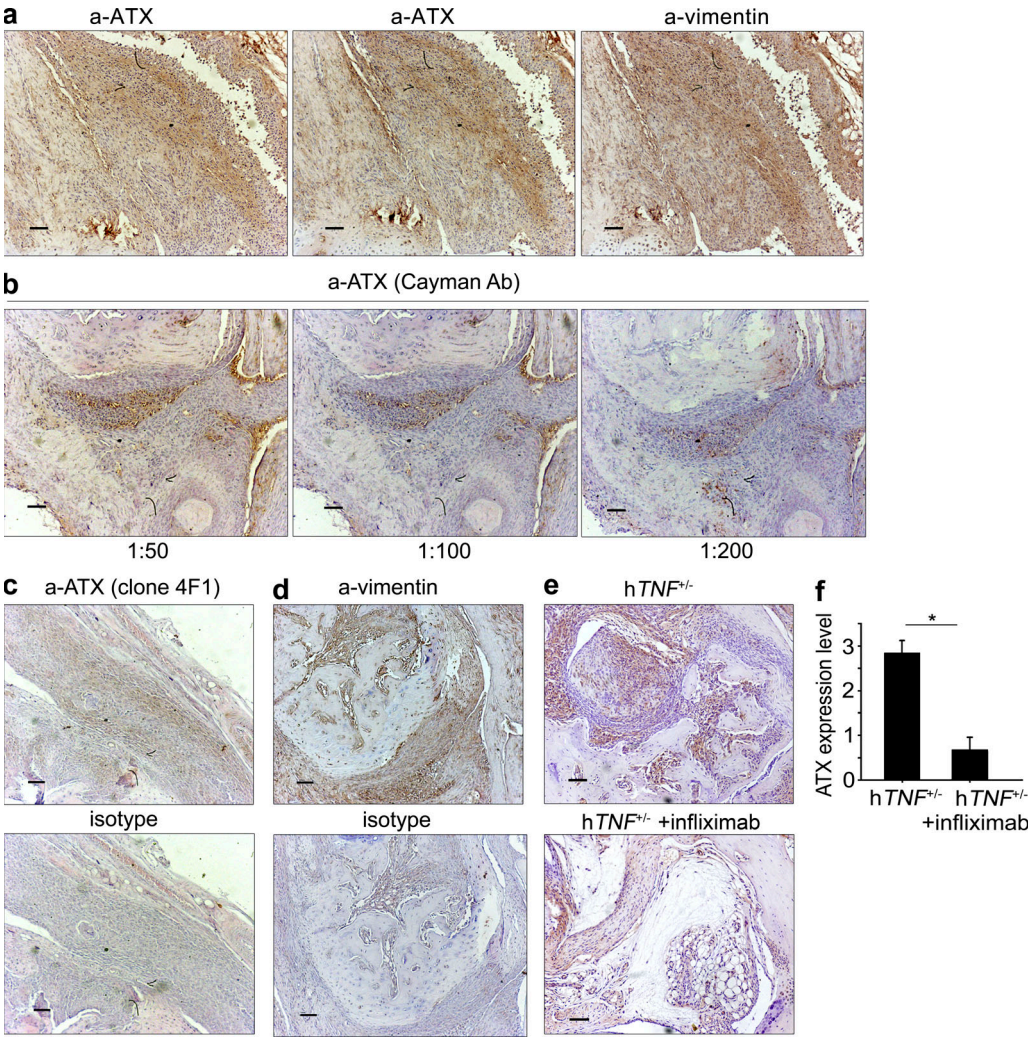

Figure S1. Increased, TNF-driven ATX expression in mouse arthritic joints in vivo. (a) Representative staining for ATX (Phoenix Pharmaceuticals) and vimentin in adjacent sections of mouse arthritic joints. (b) Validation of ATX immunostaining in mouse arthritic joint sections using a different anti-ATX Ab (Cayman Chemical) in serial dilutions. (c) ATX immunostaining in joint sections from *hTNF*$^{+/-}$ mice using a monoclonal Ab (4F1) and its isotype control. (d) Vimentin immunohistochemistry in joint sections from *hTNF*$^{+/-}$ mice and respective isotype control. (e) ATX immunostaining in joint sections from *hTNF*$^{+/-}$ mice treated with infliximab or vehicle. (f) Quantification of ATX expression in joints from *hTNF*$^{+/-}$ mice treated with infliximab or vehicle. Expression levels were quantified as described in Materials and methods. Mean ± SE is shown. *, $P < 0.05$. Bars, 50 µm.

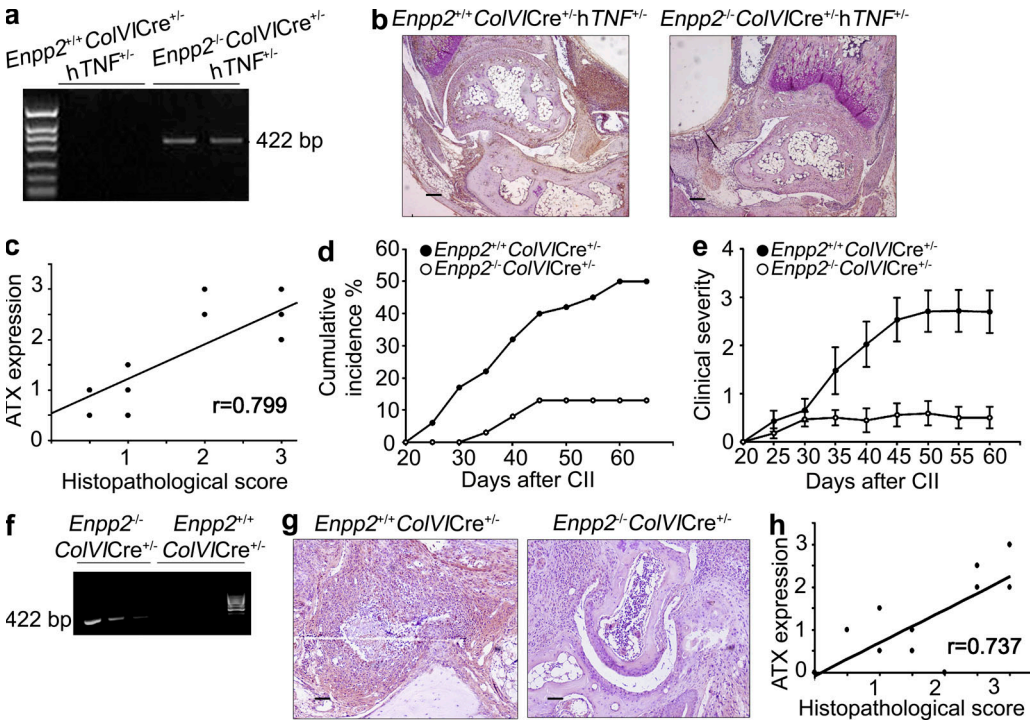

Figure S2. Genetic ablation of ATX from mesenchymal cells attenuates disease development. (a) PCR analysis of whole joint DNA extracted from paraffin block sections of the indicated mouse genetic strains confirmed correct *Enpp2* recombination. (b) Immunostaining of ATX in arthritic mouse joints of the indicated genotypes showing efficient recombination. (c) ATX expression in joint sections from *hTNF*$^{+/-}$ mice was quantified, as described in Materials and methods, and was correlated with the equivalent histopathological score. (d) Incidence of arthritis (shown as cumulative percentage) in *Enpp2*$^{+/+}$*ColVICre*$^{+/-}$ and *Enpp2*$^{-/-}$*ColVICre*$^{+/-}$ mice, relative to time, after primary immunization with CII. (e) Mean clinical scores (±SEM) of the indicated mice relative to time after primary immunization with CII. Statistical significances were assessed using a Mann-Whitney Rank Sum test. (f) PCR analysis of *Enpp2* recombination as in a. (g) Immunohistochemistry for ATX in joint sections from the indicated mice, showing efficient recombination. (h) Scatter plot showing the correlation of mouse histopathological score with ATX expression as in c. Bars, 50 µm.

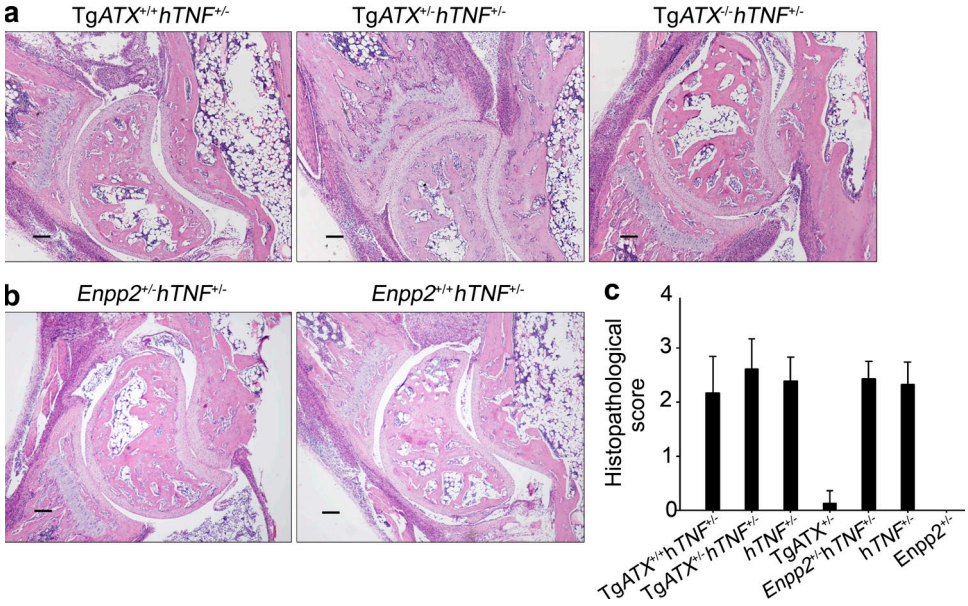

Figure S3. Systemic fluctuations of ATX do not affect arthritic disease development in the *hTNF*$^{+/-}$ animal model. (a) Representative H&E joint sections of *hTNF*$^{+/-}$ arthritic mice, carrying an ATX transgene driven by the *a1t1* promoter (in homozygosity, Tg*ATX*$^{+/+}$; or heterozygosity, Tg*ATX*$^{+/-}$). (b) Representative H&E joint sections from *hTNF*$^{+/-}$ mice after crossing with the complete heterozygous KO mouse for ATX (*Enpp2*$^{+/-}$). (c) Quantitative assessment of disease severity in all the groups of mice shown in a and b. Data are expressed as the mean ± SD (n = 5–10). Bars, 50 µm.

Table S1. Personal and clinical data of patients used for determination of ATX levels, showing a statistically significant increase of ATX in RA sera

Sample no.	Age	Gender	Diagnosis	DAS28	RF	CRP	Anti-CCP	Medication	ATX
	yr				*IE/ml*	*mg/l*	*E/ml*		*ng/ml*
S5661	51	F	RA	5.7	79	4	210	Humira	1,035.26
S5640	57	F	RA	2.3	<8	<1	390	Rituximab	221.58
S5859	56	F	RA	5.5	194	11	7,429	Humira	1,317.72
S5564	57	F	RA	2.8	21	3	802	-	440.00
S5711	55	F	RA	4.9	-	<1	2,680	Humira	439.30
S5509	56	M	RA	3.7	186	4	730	Rituximab	684.04
S5620	58	M	RA	4.6	398	41	1,499	Abatacept	252.46
S5451	60	M	RA	4.9	<10	12	348	Rituximab	237.72
S5166	57	M	RA	5.2	286	15	1,263	Rituximab	1,856.49
S5749	51	M	RA	4.6	143	7	5,418	Humira	962.28
S4040	57	M	RA	-	<10	78	2	-	207.89
S4104	53	M	RA	-	-	-	1,162	-	727.54
S4120	58	M	RA	-	-	<2	-	-	550.53
S3980	50	F	RA	-	<10	11	21	-	314.56
S4006	53	F	RA	-	-	-	90	-	448.77
S4002	54	F	RA	4.1	50	5	200	-	322.81
S4021	58	F	RA	-	-	2	-	-	905.44
S4099	54	F	RA	-	-	93	-	-	1,718.95
S4121	58	F	RA	-	-	16	35	Remicade	2,454.04
S5018	56	F	RA	4.5	271	10	180	Humira	3,498.42
S5044	60	F	RA	-	92	193	1,845	Humira	237.37
S5220	50	F	RA	4.2	<10	1	1	Rituximab	311.40
S 5661	51	F	RA	5.7	79	4	210	Humira	893.16
S 5605	56	M	RA	3.8	142	8	566	Rituximab	474.91
S 6004	62	M	RA	5.2	1,850	20	1,616	Tocilizumab	2,783.33
S4110	55	F	RA	5.9	-	-	-	-	3,290.35
S3316	58	M	OA	-	-	-	-	-	151.93
S3318	58	M	OA	-	-	-	-	-	182.98
S3357	57	M	OA	-	-	-	-	-	200.53
S3362	57	F	OA	-	-	-	-	-	170.88
S3409	60	F	OA	-	-	-	-	-	447.54
S3411	53	F	OA	-	-	-	-	-	157.89
S3414	54	M	OA	-	-	-	-	-	130.35
S3413	56	F	OA	-	-	-	-	-	117.37
S3416	57	M	OA	-	-	-	-	-	176.49
S3419	51	F	OA	-	-	-	-	-	511.40
S3249	50	F	OA	-	-	-	-	-	566.84
S3353	53	F	OA	-	-	-	-	-	268.07
S3400	50	F	OA	-	-	-	-	-	235.79
S3419	52	F	OA	-	-	-	-	-	105.79
S3468	53	F	OA	-	-	-	-	-	384.74
S3562	54	F	OA	-	-	-	-	-	234.56
S3643	56	F	OA	-	-	-	-	-	366.84
S3580	58	F	OA	-	-	-	-	-	788.95
S3334	54	M	OA	-	-	-	-	-	717.19
S3641	54	M	OA	-	-	-	-	-	246.84
S3533	52	M	OA	-	-	-	-	-	232.81
S3521	59	M	OA	-	-	-	-	-	573.86
S3485	59	M	OA	-	-	-	-	-	255.44
OAS004	63	F	OA	-	-	1.5	-	-	203.68

Table S1. Personal and clinical data of patients used for determination of ATX levels, showing a statistically significant increase of ATX in RA sera *(Continued)*

Sample no.	Age	Gender	Diagnosis	DAS28	RF	CRP	Anti-CCP	Medication	ATX
OAS015	57	M	OA	-	-	10	-	-	121.23
OAS016	65	F	OA	-	-	0.8	-	-	239.12

As shown in Fig. 3 f. DAS28, RF, CRP, and anti-CCP were estimated at the same date (±2 d). "–" denotes unavailable data.

Table S2. Personal and clinical data of patients used for determination of ATX levels, showing a statistically significant increase of ATX in RA synovial fluids

Sample no.	Age	Gender	Diagnosis	DAS28	RF	CRP	Anti-CCP	Medication	ATX
	yr				*U/ml*	*mg/l*	*E/ml*		*ng/ml*
SF676	57	M	RA	-	2,140	58	-	-	6,645.97
SF624	40	F	RA	-	-	14	-	-	8,396.42
SF669	41	F	RA	-	22	4	-	-	5,866.27
SF657	48	F	RA	7.8	-	<2	-	-	7,057.91
SF675	65	M	RA	-	81	3	-	-	6,900.30
SF673	45	F	RA	6.5	332	131	-	-	7,608.36
SF729	58	F	RA	-	-	-	-	-	7,882.99
SF692	72	M	RA	-	-	3	-	-	5,672.84
SF712	55	F	RA	-	-	12	-	Remicade	6,240.00
SF793	35	F	RA	7.5	192	7	-	Humira	5,826.87
SF757	47	M	RA	-	<10	<2	1	Remicade	6,690.15
SF746	46	F	RA	6.5	240	54	-	-	12,255.52
SF743	45	F	RA	-	<10	63	2	Remicade	5,909.25
SF771	71	F	RA	5.7	-	56	-	-	10,060.90
SF765	59	M	RA	7	-	-	-	-	5,799.40
SF794	50	F	RA	7.6	92	193	1,845	Humira	5,619.10
SF588	57	F	OA	-	-	-	-	-	4,746.27
SF792	60	F	OA	-	-	-	-	-	5,374.33
SF795	77	F	OA	-	-	-	-	-	6,567.16
SF803	71	F	OA	-	-	-	-	-	4,234.03
SF807	74	M	OA	-	-	-	-	-	5,732.54
SF596	72	F	OA	-	-	-	-	-	6,241.19
SF648	53	F	OA	-	-	-	-	-	6,107.46
SF805	65	F	OA	-	-	-	-	-	4,808.36
SF806	80	F	OA	-	-	-	-	-	5,612.40

As shown in Fig. 3 g. DAS28, RF, CRP, and anti-CCP were estimated at the same date (±2 d). "–" denotes unavailable data.